Preprint typeset using LaTeX style emulateapj v. 14/09/00

THE $L_X - \sigma$ RELATION FOR GALAXIES AND CLUSTERS OF GALAXIES

Andisheh Mahdavi[1] and Margaret J. Geller[2]
Harvard-Smithsonian Center for Astrophysics, MS 10, 60 Garden St., Cambridge, MA 02138, USA
Submitted April 4, 2001, and accepted May 15, 2001 for publication in The Astrophysical Journal Letters

ABSTRACT

We demonstrate that individual elliptical galaxies and clusters of galaxies form a continuous X-ray luminosity—velocity dispersion ($L_X - \sigma$) relation. Our samples of 280 clusters and 57 galaxies have $L_X \propto \sigma^{4.4}$ and $L_X \propto \sigma^{10}$, respectively. This unified $L_X - \sigma$ relation spans 8 orders of magnitude in L_X and is fully consistent with the observed and theoretical luminosity—temperature scaling laws. Our results support the notion that galaxies and clusters of galaxies are the luminous tracers of similar dark matter halos.

Subject headings: Galaxies: clusters: general — X-rays: galaxies

1. INTRODUCTION

X-ray observations of galaxy clusters show that gas and dark matter halos dominate the gravitational potentials of these 10^{12}–$10^{16} M_\odot$ systems. Measurements of the temperature and luminosity of the gas can probe the mass spectrum of clusters and thus provide a test of cosmological models (Markevitch 1998; Henry 2000). Crucial to these tests is the idea that clusters are a homologous set of objects with simple physical properties: that the least massive clusters are essentially the same kind of object as the gargantuan, and that simple scaling laws link observables such the X-ray luminosity L_X, temperature T, and the galaxy velocity dispersion σ for clusters of all masses.

Basic theoretical models, which assume hydrostatic equilibrium among the gas, galaxy, and dark matter components, yield $L_X \propto T^2 \propto \sigma^4$ for bremsstrahlung-dominated emission (Quintana & Melnick 1982; Eke et al. 1998). Observational tests of these models reveal several discrepancies. First, for many samples of clusters, data from both the *Einstein* and *ROSAT* satellites yields $L_X \propto T^{2.5-3} \propto \sigma^{4-5}$ (Mushotzky & Scharf 1997; Mulchaey & Zabludoff 1998). Various mechanisms—the systematic variation of the cluster baryon fraction with T (David et al. 1993), or cooling flows (Allen & Fabian 1998)—may be responsible for the overall difference in slope.

A further complication, however, is that the deviations from the simple theoretical models appear to depend on T and σ, and thus break the supposed self-similarity of galaxy clusters. A smooth transition from $L_X \propto T^{2.5}$ to $L_X \propto T^5$ occurs around $kT \lesssim 2$ keV (Ponman et al. 1996; Helsdon & Ponman 2000), possibly because of nongravitational heating of the cluster gas due to, e.g., supernova explosions or shocks (Kaiser 1991; Cavaliere, Menci, & Tozzi 1998; Tozzi, Scharf, & Norman 2000; Lloyd-Davies, Ponman, & Cannon 2000). Oddly, a similar steepening is not observed in the $L_X - \sigma$ relation (Mulchaey & Zabludoff 1998; Mahdavi et al. 2000).

Resolving the discrepancy between these cluster scaling relations requires a much larger sample of objects with known $kT \lesssim 2$ keV and $\sigma \lesssim 350$ km s^{-1}. The obvious approach is to undertake an extensive search for poor groups of galaxies; here we include two recent surveys for X-ray emission from these systems (Helsdon & Ponman 2000; Mahdavi et al. 2000).

Another approach is to regard individual, X-ray emitting elliptical galaxies as low-mass extensions of clusters. In N-body simulations of structure formation, dark matter halos are a single class of objects regardless of mass; galaxies and clusters are just luminous tracers of the halos. In particular, halos in the simulations of (Navarro, Frenk, & White 1997, NFW) have density profiles with a shape independent of the halo mass. The NFW profile is consistent with kinematic data for individual elliptical galaxies (Sato et al. 2000) as well as with rich cluster data (Nevalainen, Markevitch, & Forman 2000; Geller, Diaferio, & Kurtz 1999; Rines et al. 2000). This agreement suggests that cluster and galaxy scaling laws are related. As an example, we demonstrate that galaxies and systems of galaxies form a single, well defined relation in the $L_X - \sigma$ plane. Throughout the paper we take $H_0 = 50$ km s^{-1} Mpc^{-1}.

2. SAMPLE

We construct a sample of galaxies and clusters of galaxies that is suitable for determining the shape of the $L_X - \sigma$ relation over several decades in luminosity and velocity dispersion. Because the relation is poorly constrained for the least luminous systems of galaxies ($L_X < 10^{43}$ erg s^{-1}), we have paid particular attention to increasing number of poor groups relative to previous analyses.

Our starting point is the catalog of clusters and groups assembled by Wu, Xue, & Fang (1999) and Xue & Wu (2000). They gather velocity dispersions and standardized bolometric X-ray luminosities for 251 systems from the literature. We use two recent surveys for X-ray emission from groups (Mahdavi et al. 2000; Helsdon & Ponman 2000) to provide more accurate X-ray luminosities and to add 29 generally low L_X objects to the sample. Wherever possible, we also update the velocity dispersions of systems from our ongoing deep redshift survey of poor groups (Mahdavi et al. 1999), which has a limiting magnitude $m_B = 16.5$ and which includes typically ≈ 20 members per system.

The sources for the galaxy sample are *Einstein* and

[1] amahdavi@cfa.harvard.edu
[2] mgeller@cfa.harvard.edu

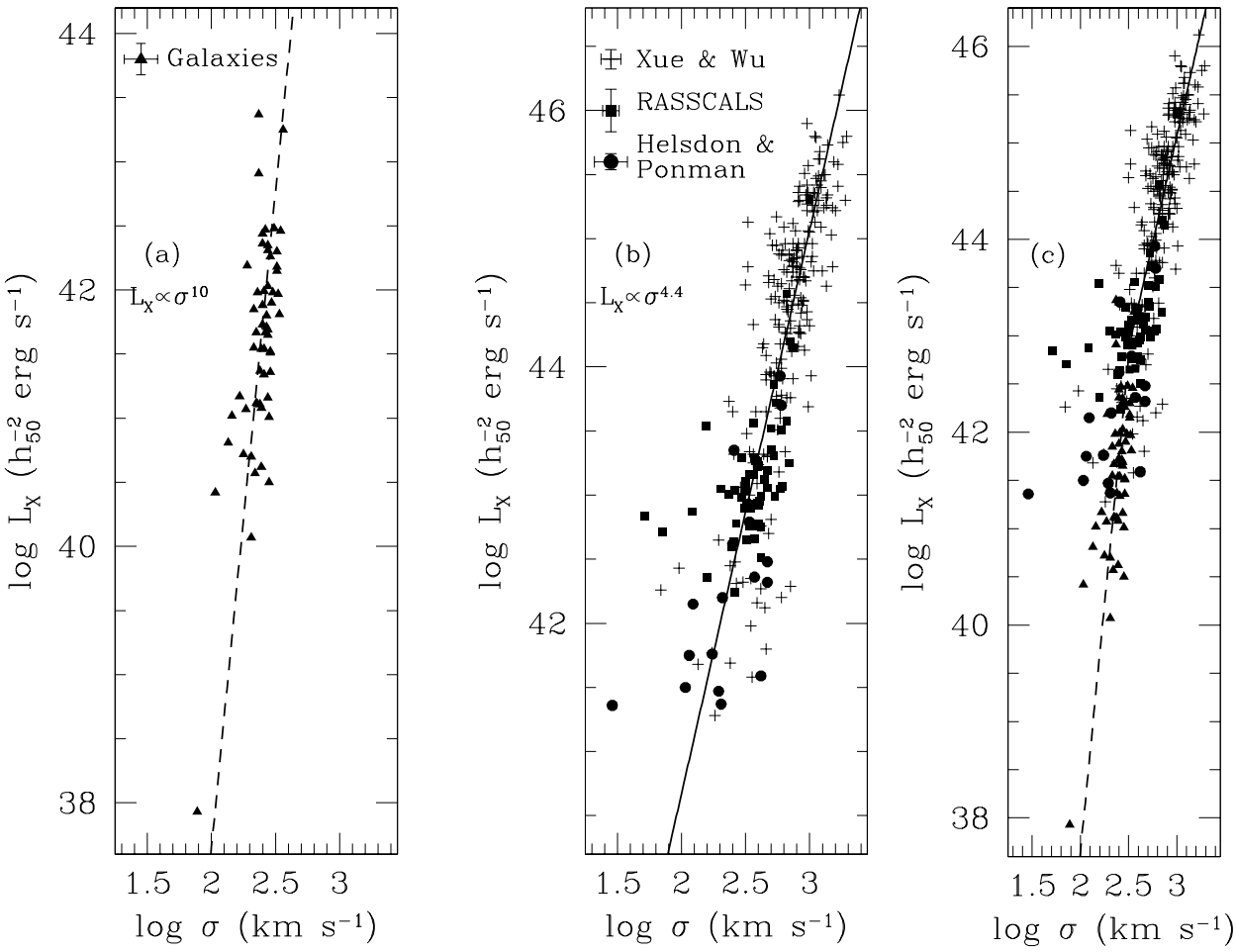

FIG. 1.— $L_X - \sigma$ relation for (a) galaxies and (b) clusters. The unified relation appears in (c). The dashed and solid lines show the best fit power laws for the galaxy and cluster samples, respectively. The error bars show the mean uncertainties in L_X and σ for each sample.

ROSAT X-ray observations by Eskridge, Fabbiano, & Kim (1995) and Beuing et al. (1999). We match the galaxies in these catalogs with the line-of-sight velocity dispersions measured by Faber et al. (1989), obtaining 84 unique objects. We exclude all galaxies containing active galactic nuclei (AGN) by comparing our sample with the AGN catalog of Veron-Cetty & Veron (2000).

Another problem is the excess X-ray emission associated with ellipticals that are the dominant central galaxies in groups (Helsdon et al. 2001). These galaxies have X-ray atmospheres that stand out from the larger intragroup emission, yet are continuous with it. In examining their *ROSAT* observations of systems containing such galaxies, Mulchaey & Zabludoff (1998) and Helsdon & Ponman (2000) argue that the X-ray emission from dominant ellipticals is linked to the gravitational potential of the whole group. We therefore exclude all galaxies in Eskridge et al. (1995) and Beuing et al. (1999) with X-ray emission associated with a cluster or group. The final sample contains 57 uncontaminated galaxies; the 27 excluded galaxies show no $L_X - \sigma$ correlation.

We have put the galaxy X-ray luminosities on the same bolometric standard as the clusters, with the assumption that the X-ray emission is due to a thermal, optically thin plasma with $kT = 1$ keV and a metallicity equal to 30% the solar value. Because none of the authors provide error estimates for the galaxy L_X and σ measurements, we assign an uncertainty of 30% to each of these quantities.

The full catalog, in which we list all 280 clusters and 84 galaxies with J2000 coordinates, redshifts, and names conforming to the NASA Extragalactic Database (NED) format, appears in Table 1, and is available electronically at http://tdc-www.harvard.edu/lxsigma, as well as in the arXiv source distribution for this paper.

3. DISCUSSION

Here we evaluate the strength and shape of the correlation between X-ray luminosity and velocity dispersion for both clusters and individual galaxies. We model the $L_X - \sigma$ relation as a power law for each sample, and examine its consistency with the observed and theoretical gas temperature scaling laws.

To conduct a detailed statistical analysis of the two samples, we first calculate Kendall's τ as a measure of correlation between L_X and σ. We then perform linear regression in log-log space by minimizing the error-weighted orthogonal distance to the straight line; see Press et al. (1992) and Lupton (1993). The results appear in Table 2 and Figure 1.

Clusters and elliptical galaxies define power laws in the $L_X - \sigma$ plane. The galaxies have highly correlated L_X and σ (with a 10^{-5} chance of a false correlation) and a very steep $L_X \propto \sigma^{10}$. The clusters show a similarly robust correlation, but a shallower $L_X \propto \sigma^{4.4}$. Table 2 and Figure 2 show that the galaxies have a much smaller scatter around the best fit line than do the clusters.

The galaxy scatter—0.1 dex on the average—is similar to that of the X-ray fundamental plane constructed by Fukugita & Peebles (1999, FP99), who fit a relation of the form $L_X \propto \sigma^a r^b$, where r is the characteristic radius of the elliptical galaxy. Using a sample of 30 galaxies, FP99 show that the best fit a and b range from $0.8 - 4.0$ and $0.6 - 2.3$ respectively, depending on the data which determine r (X-ray or optical). The discrepancy between their a and the $L_X - \sigma$ slopes in Table 2 results from the strong correlation between r and the total system mass.

In contrast to the tightness of the galaxy $L_X - \sigma$ relation, the behavior of the poorest clusters of galaxies is puzzling. Groups with $L_X \lesssim 10^{43}$ erg s^{-1} show only a weak correlation in the $L_X - \sigma$ plane ($\tau = 0.2$, with a 1% chance of a false result). The scatter in the cluster $L_X - \sigma$ relation falls from 0.252 dex to 0.182 dex when we exclude poor groups. The groups with the largest fit residuals tend to be too bright for their velocity dispersions, an effect previously described by dell'Antonio, Geller, & Fabricant (1994) and Mahdavi et al. (2000).

The large scatter in the $L_X - \sigma$ relation for galaxy groups may result from a nonequilibrium galaxy velocity distribution or from unresolved sources within the intragroup gas. *XMM* observations of the compact group HCG 16 (Turner et al. 2001), for example, show that the bulk of the X-ray emission from this system is associated with the individual galaxies; a robust estimate of L_X for systems like HCG 16 depends on a careful separation of the diffuse intragroup plasma from the galaxy emission. Thus deep optical redshift surveys and high resolution X-ray observations of more galaxy groups are necessary to reveal the nature of the large scatter in the $L_X - \sigma$ relation.

The unified $L_X - \sigma$ relation (Figure 1c) is physically consistent with the $L_X - T$ and $\sigma - T$ relations for individual ellipticals and systems of galaxies. According to the cluster compilation of Xue & Wu (2000),

$$L_X \propto T^{2.8\pm0.1} \text{ for } L_X > 10^{43} \text{ ergs}^{-1}; \quad (1)$$

$$L_X \propto T^{5.6\pm1.8} \text{ for } L_X < 10^{43} \text{ ergs}^{-1}; \quad (2)$$

$$T \propto \sigma^{1.5\pm0.2} \text{ for all } T \quad (3)$$

A compilation of elliptical galaxy temperatures by Davis & White (1996) has $T \propto \sigma^{1.45\pm0.2}$, consistent with the cluster result. Eliminating T from the above relations yields $L_X \propto \sigma^{4.2\pm0.4}$ and $L_X \propto \sigma^{8.4\pm2.9}$ for systems above and below the 10^{43} erg s^{-1} break. These predictions match the results of our analysis (Table 2).

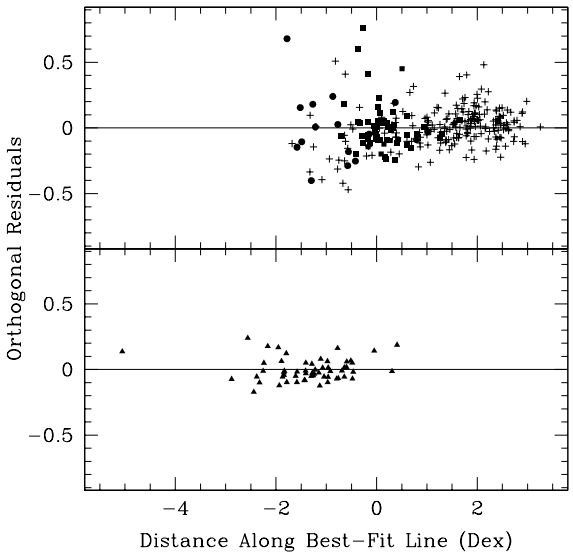

FIG. 2.— (a,b) Orthogonal $L_X - \sigma$ residuals for clusters (top) and individual galaxies (bottom). The zero point of the x-axis corresponds to the intersection of the two best-fit power laws at $\sigma = 330$ km s^{-1}, $L_X = 10^{43}$ erg s^{-1}.

Differences in the gas content of ellipticals are a concern in interpreting these relations. The *Einstein* and *ROSAT* observations of X-ray faint ellipticals—those with the lowest ratios of X-ray to optical luminosity—are probably dominated by integrated, unresolved emission from low-mass X-ray binaries (LMXB). For example, *Chandra* observations of NGC 4697 resolve 60% of the emission into LMXBs, with another 20% due to unresolved LMXBs and only 20% of the emission due to the interstellar gas (Sarazin, Irwin, & Bregman 2000). On the other hand, the bulk of the emission in the brightest ellipticals is from the hot ISM. Because both the gas content and the number of LMXBs of a galaxy should be related to its total mass, it is not surprising that we observe a tight $L_{\rm X}-\sigma$ relation despite these physical differences.

Here we attempt to adjust the $L_{\rm X}-\sigma$ relation for differences in the contribution of the galaxy ISM to the total X-ray luminosity. We assume that the total X-ray emission fraction from the ISM, $f_{\rm ISM}$, (1) is a function of the X-ray to optical emission ratio, $L_{\rm X}/L_{\rm B}$, and (2) is anchored at 20% by NGC 4697 and at 99% by NGC 5044, the brightest uncontaminated galaxy in our sample, where the emission is almost entirely from the hot ISM (Buote 2000). Using the $L_{\rm X}/L_{\rm B}$ data in Eskridge et al. (1995), these assumptions yield

$$f_{\rm ISM} \propto \left(\frac{L_{\rm X}}{L_{\rm B}}\right)^{0.3\pm0.1}. \qquad (4)$$

Eskridge et al. (1995) observe a significant correlation between the X-ray luminosity and X-ray to optical emission ratio: $L_{\rm X}/L_{\rm B} \propto L_{\rm X}^{0.56\pm0.04}$. Combining this result with equation (4) and our $L_{\rm X}-\sigma$ fit, we find

$$L_{\rm ISM} = f_{\rm ISM} L_{\rm X} \propto L_{\rm X}^{1+0.56\times0.3} \propto \sigma^{12\pm5}. \qquad (5)$$

We conclude that the variation in the gas content of elliptical galaxies has only a mild effect on the galaxy $L_{\rm X}-\sigma$ relation, steepening it within the measured uncertainties.

4. CONCLUSION

Clusters of galaxies and elliptical galaxies form a continuous, well-defined relation in the $L_{\rm X}-\sigma$ plane. The best-fit power laws have the form $L_{\rm X} \propto \sigma^m$, with $m = 4.4^{+0.7}_{-0.3}$ and $m = 10.2^{+4.1}_{-1.6}$ respectively, intersecting at $\sigma = 330$ km s^{-1}, $L_{\rm X} = 10^{43}$ erg s^{-1}. The steepening of the $L_{\rm X}-\sigma$ relation from clusters to individual galaxies supports models where the gaseous medium is preheated by supernova explosions or merging shocks, and is consistent with the observed $L_{\rm X}-T$ and $\sigma-T$ relations for galaxies and systems of galaxies. The systematic variation in the gas content of elliptical galaxies has a negligible effect on these results.

The scatter in the $L_{\rm X}-\sigma$ relation is smallest at the scale of objects which are more likely to have reached dynamical equilibrium—rich clusters of galaxies and individual ellipticals. Poor groups of galaxies have the largest scatter, an indication that unresolved, embedded X-ray sources or a nonequilibrium galaxy velocity distribution affect the integrated properties of these systems.

We thank the anonymous referee for useful comments. This research has been supported by the Smithsonian Institution.

REFERENCES

Allen, S. W. & Fabian, A. C. 1998, MNRAS, 297, L57
Beuing, J., Dobereiner, S., Bohringer, H., & Bender, R. 1999, MNRAS, 302, 209
Buote, D. A. 2000, ApJ, 539, 172
Cavaliere, A., Menci, N., & Tozzi, P. 1998, ApJ, 501, 493+
David, L. P., Slyz, A., Jones, C., Forman, W., Vrtilek, S. D., & Arnaud, K. A. 1993, ApJ, 412, 479
Davis, D. S. & White, R. E. 1996, ApJ, 470, L35
dell'Antonio, I. P., Geller, M. J., & Fabricant, D. G. 1994, AJ, 107, 427
Eke, V. R., Navarro, J. F., & Frenk, C. S. 1998, ApJ, 503, 569
Eskridge, P. B., Fabbiano, G., & Kim, D. 1995, ApJS, 97, 141
Faber, S. M., Wegner, G., Burstein, D., Davies, R. L., Dressler, A., Lynden-Bell, D., & Terlevich, R. J. 1989, ApJS, 69, 763
Fukugita, M. & Peebles, P. J. E. 1999, ApJ, 524, L31
Geller, M. J., Diaferio, A., & Kurtz, M. J. 1999, ApJ, 517, L23
Helsdon, S. F. & Ponman, T. J. 2000, MNRAS, 315, 356
Helsdon, S. F., Ponman, T. J., O'Sullivan, E., & Forbes, D. A. 2001, MNRAS in press (astro-ph/0103293)
Henry, J. P. 2000, ApJ, 534, 565
Kaiser, N. 1991, ApJ, 383, 104
Lloyd-Davies, E. J., Ponman, T. J., & Cannon, D. B. 2000, MNRAS, 315, 689
Lupton, R. 1993, Statistics in theory and practice (Princeton, N.J.: Princeton University Press, —c1993)
Mahdavi, A., Böhringer, H., Geller, M. J., & Ramella, M. 2000, ApJ, 534, 114
Mahdavi, A., Geller, M. J., Böhringer, H., Kurtz, M. J., & Ramella, M. 1999, ApJ, 518, 69
Markevitch, M. 1998, ApJ, 504, 27
Mulchaey, J. S. & Zabludoff, A. I. 1998, ApJ, 496, 73
Mushotzky, R. F. & Scharf, C. A. 1997, ApJ, 482, L13
Navarro, J. F., Frenk, C. S., & White, S. D. M. 1997, ApJ, 490, 493
Nevalainen, J., Markevitch, M., & Forman, W. 2000, ApJ, 536, 73
Ponman, T. J., Bourner, P. D. J., Ebeling, H., & Bohringer, H. 1996, MNRAS, 283, 690
Press, W. H., Teukolsky, S. A., Vetterling, W. T., & Flannery, B. P. 1992, Numerical recipes in FORTRAN. The art of scientific computing (Cambridge: University Press, —c1992, 2nd ed.)
Quintana, H. & Melnick, J. 1982, AJ, 87, 972
Rines, K., Geller, M. J., Diaferio, A., Mohr, J. J., & Wegner, G. A. 2000, AJ, 120, 2338
Sarazin, C. L., Irwin, J. A., & Bregman, J. N. 2000, ApJ, 544, L101
Sato, S., Akimoto, F., Furuzawa, A., Tawara, Y., Watanabe, M., & Kumai, Y. 2000, ApJ, 537, L73
Tozzi, P., Scharf, C., & Norman, C. 2000, ApJ, 542, 106
Turner, M. J. L., Reeves, J. N., Ponman, T. J., Arnaud, M., Barbera, M., Bennie, P. J., Boer, M., Briel, U., Butler, I., Clavel, J., Dhez, P., Cordova, F., Dos Santos, S., Ferrando, P., Ghizzardi, S., Goodall, C. V., Griffiths, R. G., Hochedez, J. F., Holland, A. D., Jansen, F., Kendziorra, E., Lagostina, A., Laine, R., La Palombara, N., Lortholary, M., Mason, K. O., Molendi, S., Pigot, C., Priedhorsky, W., Reppin, C., Rothenflug, R., Salvetat, P., Sauvageot, J., Schmitt, D., Sembay, S., Short, A., Strüder, L., Trifoglio, M., Trümper, J., Vercellone, S., Vigroux, L., Villa, G., & Ward, M. 2001, A&A, 365, L110
Veron-Cetty, M. P. & Veron, P. 2000, European Southern Observatory Scientific Report, 19, 1+
Wu, X., Xue, Y., & Fang, L. 1999, ApJ, 524, 22
Xue, Y. & Wu, X. 2000, ApJ, 538, 65

TABLE 1
CLUSTER AND GALAXY CATALOG

NED Object[a]	RA J2000			DEC J2000			cz km s^{-1}	$\log\sigma$ km s^{-1}		$\log L_X$[b] h_{50}^{-2} erg s^{-1}		Comments [c]
Clusters												
ABELL2717	00	02	59.4	-36	02	06	0.049	2.73	0.04	44.37	0.07	
ABELL2721	00	06	14.5	-34	42	51	0.115	2.91	0.04	44.93	0.09	
ABELL2734	00	11	20.1	-28	52	19	0.062	2.80	0.04	44.76	0.06	
ABELL13	00	13	38.5	-19	30	19	0.094	2.95	0.04	44.70	0.10	
ABELL2744	00	14	19.5	-30	23	19	0.308	3.29	0.07	45.80	0.10	
SRGB062	00	18	25.2	+30	04	13	0.023	2.59	0.05	43.26	0.14	R S34-115
CL0016+1609	00	18	33.3	+16	26	36	0.541	3.09	0.05	45.45	0.05	CL0016+16
ABELL21	00	20	30.8	+28	37	39	0.095	2.79	0.13	44.91	0.09	
SRGB063	00	21	38.4	+22	24	20	0.019	2.53	0.05	43.16	0.18	R S49-1479
ZWCL0024.0+1652	00	26	36.0	+17	08	36	0.390	3.13	0.08	44.63	0.09	CL0024+16
SRGB075	00	41	15.3	+25	28	54	0.015	1.71	0.13	42.84	0.22	R
ABELL85	00	41	37.8	-09	20	33	0.056	2.91	0.04	45.29	0.03	
ABELLS0084	00	49	18.8	-29	31	36	0.110	2.52	0.06	44.78	0.08	S84
ABELL115	00	55	59.5	+26	19	14	0.197	3.07	0.13	45.49	0.10	
ABELL119	00	56	21.4	-01	15	47	0.044	2.94	0.07	44.86	0.05	
NGC315GRP	00	58	25.0	+30	39	11	0.016	2.09	0.13	42.15	0.15	H
NGC383GRP	01	00	41.2	+32	11	23	0.017	2.67	0.13	43.31	0.13	
ABELL133	01	02	39.0	-21	57	15	0.057	2.87	0.05	44.82	0.05	
SRGB087	01	04	29.8	-00	44	52	0.018	2.42	0.08	42.24	0.33	R
NGC383GRP	01	07	27.7	+32	23	59	0.017	2.72	0.03	43.31	0.02	HR S34-111 SRGB090
ABELL151	01	08	52.3	-15	25	01	0.053	2.85	0.04	44.36	0.07	
APMCC147	01	08	57.9	-46	07	50	0.023	3.01	0.05	43.93	0.01	CL0107−46
ABELL2877	01	09	49.3	-45	54	02	0.025	2.87	0.03	43.91	0.07	
ABELL154	01	10	58.1	+17	39	56	0.064	2.93	0.11	44.26	0.02	
ABELL160	01	12	51.4	+15	30	54	0.045	2.76	0.13	43.94	0.13	
SS2B037	01	13	53.2	-31	44	21	0.018	2.47	0.06	42.98	0.10	R
ABELL168	01	15	09.8	+00	14	51	0.045	2.64	0.03	44.18	0.07	
S34-113	01	23	19.1	+33	21	39	0.019	2.81	0.04	43.34	0.13	
ABELL189	01	23	40.4	+01	38	38	0.033	2.41	0.12	43.32	0.10	
NGC524GRP	01	24	01.6	+09	27	37	0.008	2.31	0.13	41.37	0.11	H
ABELL193	01	25	07.3	+08	41	36	0.049	2.86	0.04	44.48	0.09	
NGC533GRP	01	25	29.1	+01	48	17	0.018	2.61	0.04	42.95	0.02	RH SRGB102
ABELL194	01	25	33.1	-01	30	25	0.018	2.53	0.06	43.34	0.08	
SRGB103	01	26	01.3	-01	22	02	0.017	2.60	0.04	43.23	0.05	R
HCG12	01	27	33.7	-04	40	14	0.049	2.43	0.13	42.31	0.08	
SS2S056	01	36	54.4	-14	01	22	0.038	2.67	0.09	43.06	0.14	R
ABELL222	01	37	27.4	-12	58	45	0.213	2.76	0.13	44.88	0.02	
SRGB115	01	49	15.1	+13	04	09	0.016	2.49	0.08	42.90	0.10	R
ABELL262	01	52	50.4	+36	08	46	0.016	2.72	0.03	43.93	0.04	
ABELL272	01	55	19.1	+33	56	41	0.088	2.84	0.10	44.87	0.09	
SRGB119	01	56	21.6	+05	37	04	0.018	2.57	0.05	42.66	0.03	HR S49-140 NGC741GRP
HCG15	02	07	39.0	+02	08	18	0.023	2.66	0.13	41.80	0.12	
HCG16	02	09	31.3	-10	09	31	0.013	2.13	0.13	41.68	0.06	
SS2B085	02	29	12.8	-10	51	20	0.014	2.20	0.11	42.36	0.26	R
SRGB145	02	31	48.0	+01	16	27	0.022	2.59	0.05	42.94	0.31	R
ABELL370	02	39	50.5	-01	35	08	0.375	3.13	0.06	45.32	0.04	
SS2B101	02	49	34.1	-31	11	10	0.021	2.58	0.06	43.27	0.06	R ABELLS301
SRGB155	02	52	48.7	-01	17	02	0.023	2.47	0.05	43.29	0.20	R
WBL088	02	54	32.2	+41	35	10	0.017	2.94	0.05	44.48	0.07	AWM7
A400	02	57	37.4	+06	00	45	0.023	2.74	0.05	43.72	0.05	R SRGB161
ABELL399	02	57	56.4	+13	00	59	0.072	2.98	0.03	45.90	0.05	
ABELL401	02	58	56.9	+13	34	56	0.074	3.06	0.03	45.42	0.04	
ABELL407	03	01	43.7	+35	49	48	0.046	2.78	0.13	44.06	0.11	
SS2B110	03	04	11.1	-12	05	03	0.012	2.56	0.09	42.76	0.34	R

TABLE 1—*Continued*

NED Object[a]	RA J2000			DEC J2000			cz km s^{-1}	$\log\sigma$ km s^{-1}		$\log L_X$[b] h_{50}^{-2} erg s^{-1}		Comments [c]
MS0302.5+1717	03	05	19.0	+17	28	38	0.425	2.81	0.06	44.96	0.05	MS0302+16
ABELL3093	03	10	52.0	-47	23	43	0.083	2.64	0.07	43.32	0.04	
ABELL3112	03	17	52.4	-44	14	35	0.075	2.74	0.06	45.17	0.04	
ABELL426	03	18	36.4	+41	30	54	0.018	3.11	0.03	45.50	0.01	
S49-142	03	20	43.7	-01	03	07	0.021	1.84	0.01	42.26	0.14	
ABELL3126	03	28	43.7	-55	42	44	0.086	3.02	0.06	44.86	0.07	
ABELL3128	03	30	34.6	-52	33	12	0.060	2.92	0.02	44.68	0.04	
ABELL3158	03	42	39.6	-53	37	50	0.060	2.99	0.03	45.06	0.03	
ABELL458	03	45	50.6	-24	16	42	0.106	2.87	0.04	44.78	0.09	
ABELL400	03	55	33.3	-36	34	18	0.320	2.78	0.05	43.78	0.09	
ABELL3223	04	08	34.5	-30	49	08	0.060	2.81	0.04	44.27	0.01	
ABELL478	04	13	20.7	+10	28	35	0.088	2.96	0.10	45.51	0.06	
NGC1587GRP	04	30	46.1	+00	24	25	0.012	2.03	0.13	41.50	0.18	H
ABELL3266	04	31	11.9	-61	24	23	0.059	3.06	0.03	45.22	0.02	
ABELL496	04	33	37.1	-13	14	46	0.033	2.84	0.05	44.83	0.04	
MS0440.5+0204	04	43	09.7	+02	10	19	0.190	2.78	0.04	44.87	0.06	MS0440+02
ABELL514	04	47	40.0	-20	25	44	0.071	2.95	0.04	44.51	0.08	
MS0451.6-0305	04	54	10.9	-03	01	07	0.550	3.14	0.03	45.73	0.13	MS0451+02
ABELL520	04	54	19.0	+02	56	49	0.199	2.99	0.03	45.57	0.10	
ABELLS0506	05	01	04.4	-24	24	41	0.320	3.11	0.10	45.24	0.03	CL0500−24
HCG33	05	10	47.9	+18	02	05	0.026	2.24	0.13	41.77	0.11	
ABELL539	05	16	35.1	+06	27	14	0.028	2.92	0.04	44.27	0.05	
ABELL3360	05	40	18.8	-43	23	31	0.085	2.92	0.05	44.32	0.04	
ABELL548	05	47	01.7	-25	36	59	0.042	2.93	0.03	44.42	0.13	
ABELL3376	06	00	43.6	-40	03	00	0.046	2.86	0.04	44.67	0.04	
ABELL3389	06	21	47.4	-64	57	35	0.027	2.77	0.04	43.68	0.03	
ABELL3391	06	26	15.4	-53	40	52	0.051	2.90	0.04	44.70	0.04	
ABELL3395	06	27	31.1	-54	23	58	0.051	2.92	0.02	44.77	0.03	
ABELL569	07	09	10.4	+48	37	10	0.020	2.51	0.09	43.48	0.09	
ABELL576	07	21	24.1	+55	44	20	0.039	2.98	0.04	44.43	0.07	
ABELL578	07	25	01.3	+66	59	07	0.087	2.90	0.13	44.78	0.03	
NGC2276GRP	07	43	05.5	+85	22	30	0.006	2.40	0.13	43.65	0.13	NGC2300
NGC2563GRP	08	20	24.4	+21	05	46	0.016	2.53	0.13	42.79	0.02	H
ABELL671	08	28	29.3	+30	25	01	0.050	3.00	0.13	44.32	0.09	
ABELL665	08	30	45.2	+65	52	55	0.182	3.08	0.13	45.62	0.07	
NRGB004	08	38	11.5	+25	07	00	0.029	2.19	0.05	43.54	0.14	R
ZWCL0839.9+2937	08	42	56.5	+29	27	59	0.194	2.87	0.06	44.96	0.06	MS0839+29
HCG35	08	45	19.5	+44	31	18	0.054	2.54	0.13	42.35	0.11	
ABELL744	09	07	17.6	+16	39	53	0.073	2.91	0.07	44.27	0.03	
ABELL754	09	08	50.1	-09	38	12	0.054	3.03	0.10	45.36	0.03	
ABELL750	09	09	06.7	+11	01	48	0.180	3.28	0.03	45.30	0.09	
HCG37	09	13	35.6	+30	00	51	0.022	2.65	0.06	42.12	0.06	
NRGS027	09	16	06.2	+17	36	08	0.029	2.59	0.06	43.22	0.18	R
A779	09	19	48.0	+33	45	32	0.023	2.57	0.04	43.29	0.14	R NRGB032
NRGS038	09	23	35.0	+22	19	58	0.031	2.79	0.04	43.07	0.24	R
N45-384	09	27	51.8	+30	01	55	0.027	2.38	0.13	42.45	0.12	
NRGB045	09	33	27.1	+34	03	02	0.027	1.85	0.11	42.71	0.42	R
ABELL851	09	42	56.6	+46	59	22	0.407	3.03	0.08	45.21	0.02	
HCG42	10	00	13.1	-19	38	24	0.013	2.32	0.13	42.20	0.03	H NGC3091
NRGS076	10	06	41.8	+14	25	49	0.030	2.51	0.04	42.94	0.30	R
ZWCL1006.1+1201	10	08	46.4	+11	47	16	0.221	2.96	0.05	44.96	0.07	MS1006+12
MS1008.1-1224	10	10	34.1	-12	39	48	0.301	3.02	0.04	44.96	0.06	MS1008−12
NRGB078	10	13	53.5	+38	44	24	0.023	2.53	0.05	42.76	0.52	R N56-393
ABELL957	10	13	57.3	-00	54	54	0.044	2.82	0.05	44.26	0.08	
ABELL963	10	17	09.6	+39	01	00	0.206	3.04	0.14	45.35	0.08	
NGC3258GRP	10	23	32.8	-34	45	30	0.010	2.60	0.13	43.24	0.03	
HYDRACLUSTER	10	36	51.3	-27	31	35	0.013	2.79	0.03	43.91	0.04	A1060

TABLE 1—*Continued*

NED Object[a]	RA J2000			DEC J2000			cz km s^{-1}	$\log\sigma$ km s^{-1}		$\log L_X$[b] h_{50}^{-2} erg s^{-1}		Comments [c]
HCG48	10	37	45.6	-27	04	50	0.009	2.55	0.13	41.58	0.14	
ABELL1069	10	39	54.3	-08	36	40	0.065	2.56	0.11	44.33	0.10	
SS2B153	10	50	26.9	-12	50	26	0.015	2.31	0.13	43.05	0.07	R
MS1054.4-0321	10	57	00.2	-03	37	27	0.823	3.07	0.06	45.30	0.13	MS1054−03
A1142	11	00	50.9	+10	33	17	0.035	2.70	0.05	43.35	0.20	R NRGS110
ABELL1146	11	01	20.6	-22	43	08	0.142	3.01	0.04	44.82	0.07	
A1185	11	10	31.4	+28	43	39	0.033	2.82	0.03	43.58	0.13	R NRGS117
ABELL1213	11	16	29.1	+29	15	37	0.047	2.74	0.12	43.77	0.13	
NGC3607GRP	11	17	55.9	+18	07	35	0.004	2.62	0.13	41.59	0.03	H
HCG51	11	22	21.6	+24	19	41	0.028	2.73	0.12	42.99	0.13	R NRGB128
SS2B164	11	22	43.0	-07	44	54	0.024	2.56	0.05	42.93	0.27	R
NGC3665GRP	11	23	30.6	+38	43	31	0.007	1.46	0.13	41.36	0.10	H
ABELL1300	11	32	00.7	-19	53	34	0.307	3.08	0.13	45.68	0.12	
ABELL1291	11	32	04.4	+56	01	26	0.053	2.96	0.13	44.13	0.02	
ABELL1314	11	34	48.7	+49	02	25	0.034	2.82	0.09	43.76	0.10	
HCG57	11	37	50.5	+21	59	06	0.030	2.54	0.04	41.98	0.22	
HCG58	11	42	09.4	+10	16	30	0.021	2.41	0.13	42.64	0.19	R NRGB151
A1367	11	44	44.6	+19	41	59	0.022	2.87	0.03	44.15	0.02	R NRGB155
ABELL1377	11	46	57.9	+55	44	20	0.051	2.69	0.13	43.96	0.02	
NGC4065GRP	12	04	09.5	+20	13	18	0.024	2.62	0.04	42.99	0.04	HR N79-299A NRGB177
NGC4073GRP	12	04	21.7	+01	50	19	0.020	2.78	0.13	43.70	0.01	H
N79-299	12	05	51.2	+20	32	19	0.023	2.62	0.07	42.76	0.07	
NRGB184	12	08	01.0	+25	15	13	0.023	2.54	0.09	42.90	0.12	R
ABELL1507	12	15	50.3	+59	58	20	0.060	2.37	0.13	43.73	0.14	
NGC4261GRP	12	20	02.3	+05	20	24	0.007	2.67	0.13	42.32	0.02	H
NGC4325GRP	12	23	18.2	+10	37	19	0.025	2.41	0.13	43.35	0.03	H
VIRGOCLUSTER	12	26	32.1	+12	43	24	0.004	2.83	0.03	44.18	0.01	VIRGO
MS1224.7+2007	12	27	14.9	+19	51	06	0.327	2.90	0.05	44.91	0.03	MS1224+20
MS1231.3+1542	12	33	52.4	+15	25	34	0.238	2.82	0.04	44.74	0.10	MS1231+15
N79-284	12	35	58.6	+26	55	29	0.025	2.78	0.13	42.20	0.16	
NGC4636GRP	12	42	57.2	+02	31	34	0.004	2.67	0.13	42.48	0.01	H
CENTAURUSCLUSTER	12	48	51.8	-41	18	21	0.011	2.77	0.03	44.18	0.02	A3526
SS2B187	12	50	34.1	-14	26	15	0.014	2.39	0.09	42.60	0.20	R
A1631	12	52	50.6	-15	25	37	0.015	2.65	0.12	43.12	0.08	R SS2B189
NGC4761GRP	12	52	57.9	-09	09	26	0.015	2.56	0.05	43.16	0.01	HR SS2B191 HCG62
ABELL3528	12	54	18.2	-29	01	16	0.053	2.99	0.04	43.69	0.13	
ABELL1644	12	57	14.8	-17	21	13	0.047	2.88	0.03	44.85	0.05	
ABELL3532	12	57	19.2	-30	22	13	0.055	2.87	0.06	44.74	0.06	
ABELL1651	12	59	22.9	-04	11	10	0.084	2.98	0.06	45.27	0.05	
COMACLUSTER	12	59	48.7	+27	58	50	0.023	3.00	0.02	45.31	0.01	NRGB226
ZWCL1305.4+2941	13	07	50.0	+29	25	44	0.241	2.91	0.06	44.16	0.13	CL1322+30
ABELL1689	13	11	34.2	-01	21	56	0.183	3.26	0.05	45.75	0.07	
NGC5044GRP	13	14	22.7	-16	32	04	0.008	2.56	0.13	43.25	0.13	
NRGS241	13	20	16.6	+33	08	13	0.037	2.70	0.04	43.52	0.12	R
ABELL3556	13	24	06.2	-31	39	38	0.048	2.76	0.06	44.33	0.11	
NGC5129GRP	13	24	36.0	+13	55	40	0.023	2.43	0.06	42.78	0.04	HR NRGB244
GHO1322+3027	13	24	48.2	+30	11	34	0.751	3.20	0.07	45.22	0.13	CYGNUS−A
ABELL1736	13	26	52.1	-27	06	33	0.046	2.72	0.09	44.68	0.06	
ABELL3558	13	27	54.8	-31	29	32	0.048	2.87	0.03	45.12	0.04	
NGC5171GRP	13	29	22.3	+11	47	31	0.023	2.60	0.04	42.92	0.05	HR MKW11NRGB247
SC1327-312	13	29	47.0	-31	36	29	0.050	2.76	0.09	44.50	0.13	SC1327-312
ABELL3559	13	29	53.9	-29	31	29	0.046	2.66	0.06	43.65	0.03	
ABELL3562	13	33	31.8	-31	40	23	0.049	2.87	0.03	44.79	0.05	
NRGB251	13	34	25.7	+34	40	54	0.025	2.42	0.05	43.04	0.17	R
ABELL1767	13	36	00.3	+59	12	43	0.070	2.97	0.09	44.67	0.05	
RXJ1340.6+4018	13	40	33.4	+40	17	48	0.171	2.58	0.26	43.65	0.13	
ABELL1775	13	41	55.6	+26	21	53	0.072	3.18	0.12	44.78	0.06	

TABLE 1—*Continued*

NED Object[a]	RA J2000			DEC J2000			cz km s^{-1}	$\log\sigma$ km s^{-1}		$\log L_X$[b] h_{50}^{-2} erg s^{-1}		Comments [c]
SS2S237	13	43	58.8	-19	50	32	0.033	2.62	0.10	42.75	0.31	R
ABELL3571	13	47	28.9	-32	51	57	0.039	3.02	0.04	45.26	0.03	
ABELL1795	13	49	00.5	+26	35	07	0.063	2.92	0.04	45.41	0.03	
HCG67	13	49	03.5	-07	12	20	0.024	2.38	0.13	41.69	0.10	SS2B239
ABELL1800	13	49	41.4	+28	04	08	0.075	2.86	0.13	44.84	0.06	
NGC5353GRP	13	51	37.0	+40	32	12	0.008	2.24	0.13	41.76	0.03	H
ABELL1809	13	53	18.9	+05	09	15	0.079	2.88	0.04	44.56	0.10	
HCG68	13	53	40.9	+40	19	07	0.008	2.26	0.13	41.28	0.27	
ABELL1831	13	59	10.2	+27	59	28	0.061	2.50	0.13	44.64	0.06	
ZWCL1358.1+6245	13	59	54.3	+62	30	36	0.328	2.97	0.03	45.34	0.08	MS1358+62
3C295	14	11	20.6	+52	12	09	0.464	3.22	0.09	45.41	0.05	3C295
ABELL1904	14	22	07.9	+48	33	22	0.071	2.86	0.07	44.12	0.02	
ABELL1913	14	26	51.8	+16	40	34	0.053	2.66	0.10	43.90	0.02	
NRGB302	14	28	33.1	+11	22	07	0.026	2.51	0.04	42.65	0.59	R N67-309
WBL514	14	34	00.9	+03	46	52	0.029	2.76	0.20	43.18	0.12	MKW7
ABELL1940	14	35	27.6	+55	08	58	0.140	2.73	0.11	44.55	0.03	
WBL518	14	40	43.1	+03	27	11	0.027	2.63	0.08	44.15	0.06	MKW8
N56-381	14	47	06.6	+11	35	29	0.029	2.42	0.04	42.48	0.13	
NRGS317	14	47	09.8	+13	42	23	0.030	2.50	0.05	43.11	0.30	R
CL1446+26	14	49	28.2	+26	07	57	0.370	3.17	0.13	45.03	0.08	CL1447+26
ABELL1983	14	52	44.0	+16	44	46	0.044	2.74	0.05	44.03	0.10	
ABELL1991	14	54	30.2	+18	37	51	0.059	2.82	0.11	44.47	0.07	
MS1455.0+2232	14	57	15.2	+22	20	30	0.258	3.05	0.05	45.47	0.02	MS1455+22
ABELL2009	15	00	15.2	+21	22	09	0.153	2.91	0.13	45.36	0.08	
HCG73	15	02	40.1	+23	21	13	0.045	1.98	0.13	42.43	0.11	
NGC5846GRP	15	05	47.0	+01	34	25	0.006	2.57	0.13	42.36	0.02	H
ABELL2029	15	10	58.7	+05	45	42	0.077	3.07	0.03	45.62	0.03	
ABELL2040	15	12	45.2	+07	25	48	0.046	2.66	0.12	43.94	0.02	
MS1512.4+3647	15	14	25.1	+36	36	30	0.372	2.84	0.06	44.88	0.10	MS1512+36
ABELL2052	15	16	45.5	+07	00	01	0.035	2.75	0.06	44.63	0.03	
ABELL2061	15	21	15.3	+30	39	17	0.078	2.74	0.08	44.95	0.06	
MKW03S	15	21	50.7	+07	42	18	0.045	2.78	0.04	44.65	0.05	MKW3S
ABELL2065	15	22	42.6	+27	43	21	0.073	3.04	0.12	45.13	0.05	
ABELL2063	15	23	01.8	+08	38	22	0.035	2.82	0.03	44.57	0.04	NRGS341
ABELL2069	15	23	57.9	+29	53	26	0.116	2.92	0.13	45.30	0.06	
ABELL2079	15	28	04.7	+28	52	40	0.066	2.83	0.06	44.43	0.08	
WBL574	15	32	29.3	+04	40	54	0.040	2.53	0.13	43.00	0.13	MKW9
ABELL2092	15	33	19.4	+31	08	58	0.067	2.70	0.08	43.95	0.08	
ABELL2107	15	39	47.9	+21	46	21	0.041	2.76	0.11	44.31	0.07	
ABELL2124	15	44	59.3	+36	03	40	0.066	2.91	0.04	44.49	0.10	
ABELL2142	15	58	16.1	+27	13	29	0.091	3.05	0.04	45.79	0.03	
ABELL2147	16	02	17.2	+15	53	43	0.035	3.03	0.09	44.75	0.03	
ABELL2152	16	05	22.4	+16	26	55	0.041	2.85	0.04	43.76	0.13	
ABELL2162	16	12	30.0	+29	32	23	0.032	2.56	0.07	43.32	0.10	
ABELL2163	16	15	34.1	-06	07	26	0.203	3.23	0.13	46.12	0.06	
NRGS385	16	17	15.4	+34	55	00	0.031	2.78	0.03	43.51	0.09	R
CID64	16	18	00.0	+35	06	00	0.030	2.77	0.13	43.60	0.13	ZW1615+35
NRGS388	16	23	01.0	+37	55	21	0.033	2.67	0.08	43.19	0.08	R
MS1621.5+2640	16	23	35.7	+26	33	50	0.426	2.90	0.03	44.91	0.08	MS1621+26
ABELL2197	16	28	10.4	+40	54	26	0.031	2.75	0.06	43.51	0.08	
HCG82	16	28	22.1	+32	49	25	0.036	2.85	0.13	42.29	0.14	
ABELL2199	16	28	37.0	+39	31	28	0.030	2.90	0.04	44.85	0.02	
HCG83	16	35	40.9	+06	16	12	0.053	2.70	0.13	42.81	0.12	
ABELL2218	16	35	54.0	+66	13	00	0.176	3.14	0.06	45.34	0.04	
NRGS404	16	58	02.4	+27	51	42	0.035	2.56	0.09	43.56	0.05	R
ABELL2244	17	02	44.0	+34	02	48	0.097	3.09	0.13	45.40	0.04	
ABELL2256	17	03	43.5	+78	43	03	0.058	3.13	0.02	45.26	0.02	

TABLE 1—*Continued*

NED Object[a]	RA J2000			DEC J2000			cz km s^{-1}	$\log\sigma$ km s^{-1}		$\log L_X$[b] h_{50}^{-2} erg s^{-1}		Comments [c]
ABELL2255	17	12	31.0	+64	05	33	0.081	3.09	0.05	45.09	0.02	
NGC6338GRP	17	15	21.4	+57	22	43	0.028	2.77	0.13	43.93	0.01	H N34-175
RXJ1716.6+6708	17	16	49.6	+67	08	30	0.813	3.18	0.05	45.24	0.02	RXJ1716.6+6708
ABELL2271	17	17	17.5	+78	01	00	0.058	2.66	0.13	44.09	0.03	
RXJ1736.4+6804	17	36	27.7	+68	04	31	0.026	2.46	0.13	43.06	0.13	
ABELL2280	17	43	06.6	+63	44	46	0.326	2.98	0.18	45.22	0.13	
RXJ1755.8+6236	17	55	42.8	+62	37	40	0.027	2.59	0.13	43.09	0.13	
RXJ1756.5+6512	17	56	31.5	+65	12	57	0.027	2.29	0.13	42.65	0.13	
ABELLS0805	18	47	14.4	-63	19	45	0.014	2.67	0.08	43.30	0.13	S805
HCG85	18	50	22.3	+73	21	00	0.039	2.62	0.13	42.27	0.11	
ABELL2319	19	20	45.3	+43	57	43	0.056	3.19	0.02	45.60	0.02	
HCG86	19	51	59.2	-30	49	34	0.020	2.48	0.13	42.32	0.14	
ABELL3651	19	52	10.9	-55	05	16	0.060	2.80	0.04	44.52	0.18	
ABELL3667	20	12	30.1	-56	49	00	0.056	2.99	0.02	45.36	0.08	
ABELL3693	20	34	22.0	-34	29	40	0.091	2.68	0.07	44.66	0.16	
ABELL3695	20	34	47.7	-35	49	39	0.089	2.89	0.03	45.06	0.07	
ABELL3716	20	51	16.7	-52	41	43	0.046	2.98	0.05	44.37	0.08	
ABELL3733	21	01	50.0	-28	06	54	0.038	2.78	0.06	43.99	0.10	
ABELL3744	21	07	13.8	-25	28	54	0.038	2.71	0.05	44.95	0.08	
SS2S261	21	11	34.6	-23	08	52	0.033	2.84	0.09	43.25	0.10	R
MS2137.3-2353	21	40	12.8	-23	39	27	0.313	2.98	0.13	45.42	0.06	MS2137−23
ABELL3809	21	46	57.5	-43	54	06	0.062	2.68	0.05	44.71	0.08	
ABELL2390	21	53	34.6	+17	40	11	0.228	3.04	0.02	45.80	0.10	
ABELL3822	21	54	06.2	-57	50	49	0.076	2.91	0.04	44.96	0.06	
ABELL3825	21	58	22.4	-60	23	39	0.076	2.84	0.04	44.61	0.09	
ABELL3827	22	01	49.1	-59	57	15	0.098	2.98	0.18	45.36	0.05	
ABELLS0987	22	02	23.5	-22	30	15	0.070	2.83	0.07	44.45	0.21	S987
NGC7176GRP	22	02	31.4	-32	04	58	0.009	2.29	0.13	41.47	0.11	H HCG90
ABELL2426	22	14	27.3	-10	22	05	0.098	2.52	0.07	45.13	0.06	
SRGB009	22	14	48.0	+13	50	17	0.026	2.50	0.06	43.04	0.26	R
ABELL2440	22	23	52.6	-01	35	47	0.091	3.00	0.07	45.05	0.10	
ABELL3880	22	27	49.5	-30	34	40	0.058	2.93	0.08	44.54	0.07	
ABELL3888	22	34	23.0	-37	43	29	0.151	3.12	0.03	45.50	0.07	
HCG92	22	35	57.5	+33	57	36	0.021	2.59	0.13	42.16	0.04	
ABELL3921	22	49	38.6	-64	23	15	0.094	2.69	0.09	45.04	0.06	
SRGB013	22	50	00.7	+11	40	15	0.026	2.77	0.05	43.05	0.21	R S49-146
SS2B293	22	55	09.8	-33	53	06	0.028	2.08	0.12	42.87	0.23	R
ABELLS1077	22	58	52.3	-34	46	55	0.312	3.22	0.05	45.58	0.13	AC114
ABELL2556	23	13	03.3	-21	37	40	0.086	3.10	0.09	44.75	0.18	
SRGS034	23	18	31.2	+18	41	52	0.039	2.72	0.10	43.86	0.06	R
SRGB031	23	20	11.3	+08	12	05	0.011	2.60	0.06	42.78	0.08	R
NGC7619GRP	23	20	32.1	+08	22	26	0.011	2.40	0.13	42.62	0.02	H
ABELL2589	23	24	00.5	+16	49	29	0.041	2.70	0.08	44.53	0.05	
ABELL2593	23	24	31.0	+14	38	29	0.041	2.85	0.06	44.30	0.06	
SRGB037	23	28	46.6	+03	30	49	0.017	2.62	0.06	42.51	0.44	R
ABELL4010	23	31	10.3	-36	30	26	0.096	2.80	0.08	45.09	0.14	
ABELL2626	23	36	31.0	+21	09	36	0.055	2.82	0.06	44.51	0.06	
ABELL2634	23	38	18.4	+27	01	37	0.031	2.85	0.05	44.20	0.05	SRGS040
ABELL2657	23	44	51.0	+09	08	40	0.040	2.82	0.13	44.45	0.05	
HCG97	23	47	24.0	-02	19	08	0.023	2.37	0.05	43.01	0.20	R SS2B312
ABELL4038	23	47	31.1	-28	12	10	0.030	2.95	0.06	44.52	0.03	SS2B313
ABELL2666	23	50	56.2	+27	08	41	0.027	2.68	0.07	42.70	0.09	
NGC7777GRP	23	53	33.0	+28	34	42	0.023	2.06	0.13	41.75	0.20	H
ABELL2670	23	54	10.1	-10	24	18	0.076	2.96	0.03	44.70	0.08	
ABELL4059	23	56	40.7	-34	40	18	0.048	2.93	0.11	44.76	0.04	

Galaxies

TABLE 1—*Continued*

NED Object[a]	RA J2000			DEC J2000			cz km s^{-1}	$\log\sigma$ km s^{-1}		$\log L_X$[b] h_{50}^{-2} erg s^{-1}		Comments [c]
MESSIER032	00	42	41.8	+40	51	52	0.000	1.89	0.13	37.93	0.13	E NGC0221
NGC0315	00	57	48.9	+30	21	09	0.016	2.55	0.13	42.26	0.13	E AGN
IC1625	01	07	42.8	-46	54	24	0.022	2.41	0.13	41.99	0.16	B
NGC0410	01	10	58.9	+33	09	08	0.018	2.51	0.13	42.30	0.05	B
NGC0499	01	23	11.5	+33	27	38	0.015	2.37	0.13	42.65	0.13	E GR S34-113
NGC0507	01	23	40.0	+33	15	20	0.016	2.56	0.13	43.25	0.13	E
NGC0533	01	25	31.3	+01	45	33	0.019	2.50	0.13	42.84	0.13	E GR NGC533GRP
NGC0708	01	52	46.4	+36	09	07	0.016	2.38	0.13	43.44	0.02	B GR A262
NGC0720	01	53	00.4	-13	44	18	0.006	2.39	0.13	41.54	0.13	E
NGC0741	01	56	21.0	+05	37	44	0.019	2.45	0.13	42.12	0.07	B GR SRGB119
NGC0777	02	00	14.9	+31	25	46	0.017	2.54	0.13	42.46	0.05	B
NGC1052	02	41	04.8	-08	15	21	0.005	2.31	0.13	40.91	0.13	E AGN
IC0310	03	16	42.9	+41	19	30	0.019	2.37	0.13	42.91	0.03	B
NGC1399	03	38	29.3	-35	27	01	0.005	2.49	0.13	42.48	0.13	E
NGC1395	03	38	29.6	-23	01	40	0.006	2.41	0.13	41.34	0.13	E
NGC1404	03	38	52.0	-35	35	34	0.006	2.35	0.13	41.67	0.13	E
NGC1407	03	40	11.8	-18	34	48	0.006	2.46	0.13	41.51	0.13	E
NGC1600	04	31	39.9	-05	05	10	0.016	2.51	0.13	42.15	0.13	E
NGC1573	04	35	04.1	+73	15	45	0.014	2.44	0.13	41.65	0.11	B
NGC2305	06	48	37.3	-64	16	24	0.012	2.33	0.13	41.85	0.03	B
NGC2325	07	02	40.5	-28	41	50	0.007	2.13	0.13	40.81	0.14	B
NGC2329	07	09	08.0	+48	36	56	0.019	2.43	0.13	42.43	0.06	B GR A569
NGC2340	07	11	10.8	+50	10	28	0.020	2.40	0.13	42.36	0.08	B
NGC2300	07	32	19.5	+85	42	33	0.006	2.43	0.13	41.71	0.13	E
NGC2434	07	34	51.4	-69	17	01	0.005	2.31	0.13	40.07	0.14	B
NGC2563	08	20	35.7	+21	04	04	0.015	2.42	0.13	42.32	0.13	E GR NGC2563GRP
NGC2663	08	45	08.0	-33	47	44	0.007	2.45	0.13	40.50	0.20	B
NGC2832	09	19	46.8	+33	44	59	0.023	2.56	0.13	42.94	0.13	E GR A779
NGC2974	09	42	32.9	-03	41	58	0.007	2.35	0.13	41.12	0.13	E
NGC2986	09	44	16.0	-21	16	41	0.008	2.45	0.13	41.01	0.10	B
NGC3078	09	58	24.6	-26	55	35	0.008	2.38	0.13	41.37	0.13	E
NGC3091	10	00	14.3	-19	38	13	0.013	2.46	0.13	41.44	0.09	B GR HCG42
NGC3226	10	23	27.0	+19	53	54	0.004	2.31	0.13	40.62	0.09	B AGN
NGC3258	10	28	54.1	-35	36	22	0.009	2.44	0.13	41.69	0.13	E
NGC3585	11	13	16.8	-26	45	21	0.005	2.34	0.13	40.57	0.13	E
NGC3607	11	16	54.7	+18	03	06	0.003	2.39	0.13	41.08	0.13	E
NGC3608	11	16	59.0	+18	08	55	0.004	2.31	0.13	40.70	0.13	E
NGC3862	11	45	05.0	+19	36	23	0.022	2.42	0.13	42.13	0.15	B AGN GR A1367
NGC3923	11	51	02.1	-28	48	23	0.006	2.33	0.13	41.55	0.13	E
NGC4073	12	04	27.0	+01	53	48	0.020	2.44	0.13	43.16	0.03	B GR NGC4073GRP
NGC4105	12	06	40.6	-29	45	42	0.006	2.38	0.13	41.11	0.13	E
NGC4125	12	08	05.6	+65	10	29	0.005	2.36	0.13	41.11	0.08	B
NGC4168	12	12	17.3	+13	12	18	0.008	2.26	0.13	40.50	0.13	E AGN
NGC4261	12	19	23.2	+05	49	31	0.007	2.47	0.13	41.90	0.13	E
NGC4278	12	20	06.8	+29	16	51	0.002	2.42	0.13	39.91	0.11	B AGN
NGC4291	12	20	17.7	+75	22	15	0.006	2.41	0.13	41.54	0.13	E
NGC4365	12	24	28.2	+07	19	03	0.004	2.39	0.13	40.62	0.13	E
MESSIER084	12	25	03.7	+12	53	13	0.004	2.46	0.13	41.36	0.13	E NGC4374
MESSIER086	12	26	11.7	+12	56	46	-0.001	2.40	0.13	42.44	0.13	E NGC4406
NGC4458	12	28	57.5	+13	14	31	0.002	2.03	0.13	40.42	0.13	E
MESSIER049	12	29	46.8	+08	00	02	0.003	2.46	0.13	42.26	0.13	E NGC4472
NGC4473	12	29	48.9	+13	25	46	0.007	2.25	0.13	40.72	0.13	E
MESSIER087	12	30	49.4	+12	23	28	0.004	2.21	0.13	43.08	0.01	B AGN NGC4486
MESSIER089	12	35	39.8	+12	33	23	0.001	2.42	0.13	41.12	0.13	E AGN NGC4552
NGC4636	12	42	50.0	+02	41	17	0.003	2.28	0.13	42.19	0.13	E
MESSIER060	12	43	39.6	+11	33	09	0.004	2.53	0.13	41.81	0.13	E NGC4649

TABLE 1—*Continued*

NED Object[a]	RA J2000			DEC J2000			cz km s^{-1}	$\log\sigma$ km s^{-1}		$\log L_X$[b] h_{50}^{-2} erg s^{-1}		Comments [c]
NGC4697	12	48	35.7	-05	48	03	0.004	2.22	0.13	41.17	0.13	E
NGC4696	12	48	49.3	-41	18	40	0.010	2.35	0.13	43.38	0.01	B GR CENTAURUS
NGC4760	12	53	07.2	-10	29	39	0.016	2.40	0.13	41.73	0.10	B
NGC4782	12	54	35.8	-12	34	09	0.013	2.52	0.13	41.97	0.13	E
NGC4936	13	04	17.0	-30	31	31	0.010	2.40	0.13	41.88	0.10	B
NGC5044	13	15	24.0	-16	23	06	0.009	2.37	0.13	43.37	0.13	E
NGC5077	13	19	31.6	-12	39	23	0.009	2.44	0.13	41.27	0.13	E AGN
NGC5090	13	21	12.8	-43	42	16	0.011	2.43	0.13	41.80	0.11	B
NGC5129	13	24	10.0	+13	58	36	0.023	2.44	0.13	42.35	0.10	B
NGC5216	13	32	06.9	+62	42	02	0.010	2.16	0.13	41.02	0.20	B
IC4296	13	36	39.4	-33	58	00	0.012	2.51	0.13	42.18	0.13	E
NGC5328	13	52	53.6	-28	29	16	0.016	2.44	0.13	42.03	0.07	B
NGC5419	14	03	38.3	-33	58	50	0.014	2.48	0.13	41.98	0.09	B
NGC5846	15	06	29.2	+01	36	21	0.006	2.44	0.13	42.31	0.13	E
NGC5982	15	38	39.9	+59	21	21	0.010	2.42	0.13	41.67	0.13	E
NGC6160	16	27	41.2	+40	55	36	0.032	2.37	0.13	42.63	0.06	B GR A2197
NGC6166	16	28	38.5	+39	33	06	0.030	2.51	0.13	44.30	0.02	B GR A2199
NGC6173	16	29	44.9	+40	48	42	0.029	2.42	0.13	42.47	0.15	B
NGC6868	20	09	54.1	-48	22	47	0.010	2.46	0.13	41.52	0.19	B
NGC6876	20	18	20.2	-70	51	28	0.013	2.36	0.13	41.98	0.13	E
NGC7196	22	05	55.1	-50	07	11	0.010	2.44	0.13	41.16	0.12	B
NGC7192	22	06	50.3	-64	18	56	0.010	2.27	0.13	41.07	0.14	B
NGC7385	22	49	54.7	+11	36	30	0.026	2.41	0.13	42.03	0.21	B GR SRGB013
IC1459	22	57	10.6	-36	27	44	0.006	2.49	0.13	41.21	0.13	E AGN
NGC7619	23	20	14.4	+08	12	22	0.013	2.53	0.13	42.20	0.13	E GR SRGB031
NGC7626	23	20	42.3	+08	13	02	0.011	2.37	0.13	41.70	0.13	E GR NGC7619GRP
IC5358	23	47	45.0	-28	08	27	0.029	2.29	0.13	42.03	0.07	B GR A4038
NGC7768	23	50	58.6	+27	08	50	0.027	2.38	0.13	42.11	0.14	B GR A2666

Note. — All data are from Xue & Wu (2000) and Wu et al. (1999) unless the comments specify otherwise.

[a]Alternate names are indicated in the comment field.

[b]The X-ray luminosities have been standardized to bolometric.

[c]H: X-ray luminosity from Helsdon & Ponman (2000); R: X-ray luminosity and velocity dispersion from Mahdavi et al. (2000); HR: X-ray luminosity from Helsdon & Ponman (2000), velocity dispersion from Mahdavi et al. (2000); B: data from Beuing et al. (1999); E: data from Eskridge et al. (1995); GR: galaxy is coincident with intracluster emission from the noted system; AGN: galaxy is associated with an active galactic nucleus.

TABLE 2
STATISTICAL ANALYSIS OF THE $L_X - \sigma$ RELATION

Sample	N	τ	P[a]	Slope	Intercept	Scatter[b]
Clusters	280	0.652	$< 10^{-6}$	$4.4^{+0.7}_{-0.3}$	$31.8^{+0.9}_{-2.0}$	0.252
Galaxies	84	0.283	$< 10^{-6}$	$15.3^{+6.7}_{-2.9}$	5.1^{+7}_{-16}	0.152
• Contaminated	27	0.163	0.234	···	···	
• Uncontaminated	57	0.377	10^{-5}	$10.2^{+4.1}_{-1.6}$	$17.2^{+3.8}_{-10.1}$	0.094

[a]Probability that an uncorrelated sample would give the quoted value of Kendall's τ or higher by chance.

[b]Root-mean-square orthogonal scatter in the log-log plane.